Commun.Fac.Sci.Univ.Ank.Series A2-A3
Volume 61, Number 2, Pages 181-196 (2019)
DOI: 10.33769/aupse.557951
ISSN 1303-6009 E-ISSN 2618-6462
http://communications.science.ankara.edu.tr/index.php?series=A2A3

OPERATION TESTS of the 260 MHz 1500 W SOLID STATE RF AMPLIFIER at TARLA FACILITY

Ozlem KARSLI and Evrim COLAK

ABSTRACT. Turkish Accelerator and Radiation Laboratory (TARLA) will be the first accelerator-based user facility in Turkey. The facility is under construction at the Institute of Accelerator Technologies of Ankara University. Based on the state-of-art superconducting technology, TARLA accelerator offers a multi-experimental facility providing a variety of accelerator-based radiation sources for users coming from various fields like chemistry, physics, biology, material sciences, medicine and nanotechnology. TARLA consists of two acceleration lines: the first one is the injector that provides high current continuous wave (CW) electron beam at 250 keV energy, and the second one is the main accelerator that comprises of two superconducting (SC) cryomodules separated by a bunch compressor in order to accelerate the electron beam up to 40 MeV energy. Two normal conducting accelerators, so called subharmonic (SHB) and fundamental (FB) buncher cavities whose operation frequencies are 260 and 1300 MHz, respectively, are used to compress the electron bunches from ~600 ps to ~10 ps. SHB cavity is powered by a 1500 W Radio frequency (RF) power amplifier. Currently, the electron gun training, and superconducting modules acceptance tests, personal safety system, and helium cryogenic system commissioning tests are performed simultaneously. In this study, we present the operation tests of the 1500 W RF amplifier in the scope of the commissioning tests of injector line which showed phase drift coefficients of ~0.5 deg/C^o and ~0.67 deg/C^o in repeated tests. Moreover, the importance of constancy of the water pressure in the water-cooling line for phase constancy of the delivered power has become evident as a result of current observations.

1. INTRODUCTION

Turkish Accelerator and Radiation Laboratory (TARLA) has been proposed as an oscillator mode infrared (IR) free electron laser (FEL) facility in the scope of Turkish

Received by the editors: April 26, 2019; Accepted: December 11, 2019.
Key word and phrases: Radio frequency (RF), solid state amplifier, accelerator, bunch length, phase stability, high power, operation test.

Accelerator Center (TAC) Project [1] and it is under construction since 2012 [2]. After submitting the conclusion reports of TAC project, the installation of the facility has been continuing as the TARLA project since 2016 [3].

TARLA will be the first accelerator based research center in Turkey that produces electrons up to 40 MeV with a tunable infrared free electron laser (FEL) source in 3-350 µm range with high peak (~5 MW) and high average power (~100 W), and a Bremsstrahlung radiation between 5-30 MeV energy [3]. The facility will serve four FEL experimental stations for researchers to study material science, infrared spectroscopy, biomedical, chemistry, nanotechnology and semiconductor. Additionally, researchers will have an opportunity to perform fixed target experiments with Bremsstrahlung laboratory. The schematic view of TARLA is illustrated in Fig. 1[2].

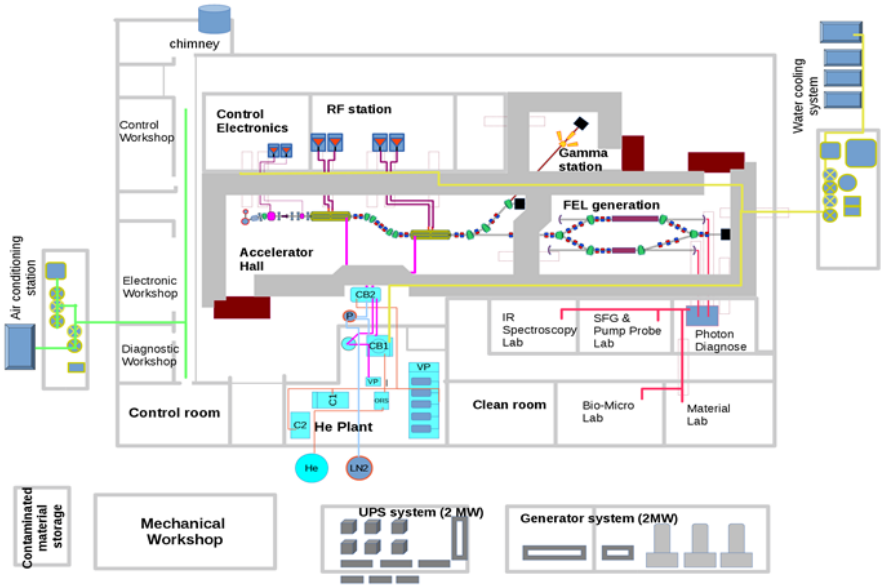

FIGURE 1. General view of TARLA facility [2].

Currently, acceptance tests of superconductive accelerator modules, commissioning tests of personal security system, and helium cooling system, electron gun training tests are carried out, simultaneously.

TARLA injector line consists of an electron gun, subharmonic buncher (SHB) and fundamental buncher (FB) cavities, a macro-pulser, and solenoid and steering magnets, in basic. Electron gun is a thermionic type of DC gun and is composed of a tungsten dispenser cathode and a grid providing a ~600 ps pulsed electron beam in 13 MHz repetition rate [4]. Electron beam should be formed into bunches in the

injector line, before entering the superconducting modules. A buncher cavity is a normal conducting accelerating cavity. It allows the particles to be either accelerated or decelerated depending on the phase difference. It also provides velocity modulation which is called as ballistic bunching [5]. TARLA injector line has a SHB and a FB that operates at frequency of 260 MHz and 1300 MHz, respectively. The longitudinal waist of electrons are formed into from ~600 ps to 10 ps by ballistic bunching in buncher cavities. A magnetic chicane, so called bunch compressor, will be located between two superconducting modules. Electron beam energy will be increased up to 40 MeV after the second cryomodule [3].

Buncher cavities match the longitudinal characteristics of electron beam before entering the superconducting modules operating at 1300 MHz [4]. SHB is powered by a 1500 W Radio Frequency (RF) power amplifier operating at 260 MHz. Basic parameters of the RF amplifier to feed the SHB are listed in Table 1 [6, 7].

TABLE 1. Basic parameters of RF amplifier feeding the SHB [6, 7].

Parameter	**Value**
Amplifier	Class AB push-pull
Operation frequency	260 MHz
Bandwidth (-3 dB)	<±5 MHz
Output power (@1 dB compression) pulse or CW	1300 W@1dB and 1500W saturated
Input / Output VSWR	<1.5 /<1.5 with measurement results
Linear gain	>61 dB (min)
Pulse length	10 us to CW
Pulse repetition rate	1 Hz to CW
Rise / Fall time	<60 ns
Phase drift coefficient	0.35 deg / ºC
Gain drift coefficient	1.2 % / K typ. Max.
Output phase change from min to max power	±10 deg (max)
System efficiency	> 55 % at 1500 W output

Three types of RF amplifiers have been used in acceleration science area: klystrons, inductive output tubes (IOT), and solid-state power amplifiers (SSA). Simple start-up and low-cost maintenance procedures, the high modularity with associated redundancy and flexibility, removal of a high-voltage and high-power circulator are the features that make solid-state RF amplifiers superior to others [8]. The solid-

state amplifiers exhibit extremely fast pulse rise and fall times, very tight pulse-to-pulse repeatability and excellent ruggedness [9].

Class B amplifiers are commonly used due to their simplicity and high efficiency. It is possible to operate in a broad range of frequency, if the wideband transformers are used. However, this type of amplifiers cause significant amount of distortion and harmonics due to the unmatched transistors and crossover distortion. Transistor mismatch can be avoided by using transistors in uniform characteristics. The crossover distortion can be reduced by both transistors being normally biased at a level that is slightly above cutoff (forward bias). The forward bias causes the circuit to operate in Class-AB mode, so both transistors are slightly 'On' during crossover. Under these conditions, the Class B amplifier is typically referred to as the Class AB amplifier [10].

Therefore, Class AB push-pull amplifiers have been chosen for TARLA as the high power RF sources. The parameters specified in Table 1 are designated by taking beam dynamic calculations and the characteristics of SHB into consideration. Gain, the logarithmic ratio of the output and the input power, is ~61 dB at minimum with 1 mW input power to feed the SHB. The electron bunch length which will be delivered from the SHB, heat load capacity of the antenna and the cooling parameters of the SHB determine the output power of the RF amplifier. The frequency and bandwidth of the RF amplifier should be the same with those of the SHB. Cooling parameters of SHB affects the operation temperature and cooling requirements of the RF amplifier. The rise and fall times in the order of nanoseconds are two of the important criteria for selecting solid-state RF amplifiers. Reduced rise and fall times of the amplifiers will increase the interaction between electron beam and RF wave in the SHB. Maximum output Voltage Standing Wave Ratio (VSWR) is found as 1.81 with the assumptions of 100 W reverse and 1.2 kW forward power. Regarding system efficiency, 55 % is a typical value for SSAs. These parameters were discussed with the manufacturers to find out whether such a SSA was producible or not. This amplifier module was manufactured by SigmaPhi [11] with a spare one and was delivered in 2017.

Phase and gain drift coefficients of RF amplifiers are of vital importance since the amplifiers are to operate in steady state without interruption for a long time period and they are expected not to be affected by ambient temperature changes.

In this study, we measure phase and magnitudes of the scattering parameters (S-parameters), namely, S_{11} and S_{21} for the 1500 W RF amplifier for long-time operation to observe the phase drift. The effect of variation in the temperature and the pressure of the cooling water system on the measured S-parameters is

investigated. Utilizing a home-made test routine written in NI LabVIEW Software [12] to automate the phase and magnitude measurements, the tests are repeated twice for 50 hours and ~180 hours and the results are compared with each other.

Section I is devoted to literature and basic description of the accelerator facility. Mathematical relationship between the phase of the RF signal and the parameters of the beam which is accelerated is discussed in Section II. We explain the measurement setup and data acquisition & controlling method in Section III. Section IV is dedicated to the presentation of the measurement data. The comparison of the results and the discussion of the effects of external factors such as cooling temperature and pressure level are discussed in Section V, i.e., the Conclusion Section.

2. Theoretical Background

Let us consider work done (ΔE) on a moving particle with charge q in a cavity, by the electrical field $\vec{\mathcal{E}}$ which applies force ($\vec{F}_e = q\vec{\mathcal{E}}$) along a path from $z = -d/2$ to $z = d/2$. Within the cavity, the acceleration field is applied along the z-direction, therefore, E_x and E_y, x- and y-components of the electric field are negligible. Given operation frequency ω and the electrical field phasor $\vec{\mathcal{E}} = E_z(z)\mathrm{e}^{\mathrm{j}\omega\mathrm{t}}$, the beam is accelerated only along the propagation direction (z-axis of the cavity). Such a particle entering the cavity at $z = -d/2$ will encounter the phase of the RF field. Then, the energy gain, i.e., the distribution in phase space, for the particle is given as the integral of applied force along the path [13]:

$$\Delta E = q\Re e\left\{\int_{-d/2}^{d/2} E_z(z)e^{j\omega t}dz\right\} \tag{1.1}$$

with

$$\omega t = \omega\frac{z}{v} + \psi_p \tag{1.2}$$

where ψ_p is the phase relative to RF and v is the speed of the particle when entering the gap, respectively. Hence,

$$\Delta E = q\Re e\left\{e^{-j\psi_p}\int_{-d/2}^{d/2} E_z(z)e^{j\omega\frac{z}{v}}dz\right\} \tag{1.3}$$

By introducing $\phi = \psi_p - \psi_i$, where ψ_i is the phase relative to initial position, one finally gets:

$$\Delta E = q\left|\int_{-d/2}^{d/2} E_z(z)e^{j\omega\frac{z}{v}}dz\right| cos\phi \tag{1.4}$$

where ϕ appears as the phase of the particle referred as the particular phase, which would yield the maximum energy for $\phi = 0$.

Thus, one can deduce the following: the energy that is transferred to the particle will decrease if $\phi > 0$, i.e., the phase difference between the RF wave powering the cavity and the particle, is greater than zero while the particle travels across the cavity. Since the beam emittance is affected by the phase change and the energy gain, $\phi > 0$ condition results in the deviation of the beam during its transport through the entire beamline as well as energy spread and emittance growth [4, 14].

ψ_p is optimized to minimize the energy spread, where $\frac{\Delta E}{E}$ is the energy spread of the particles [15]. The residual energy spread after compensation is found from the convolution of the bunch with the longitudinal wake-field and the acceleration RF [15],

$$\frac{\Delta E}{E} \approx \frac{1.25}{Gcos\psi_p}\left[KGsin\psi_p\right](FWHM) \tag{1.5}$$

where *K* is a variable depending to the electron beam and RF, and $G = qV_{RF}/m_e c^2$, where m_e is electron mass and c is the speed of light [15]. TARLA has set a design criterion for resolution in energy of the exit beam such that $\frac{\Delta E}{E} < 5x10^{-4}$.

To understand the stability of the output signal phase of the RF amplifier (RF-PA), S-parameters which give information about the phase and amplitude of the electromagnetic wave are to be examined [16]. It is defined as $S_{ij} = {V_i^-}/{V_j^+}$ for an *N*-port system ($\{N, i, j\} \in \mathbb{N}^+$) where V_i^- is the signal leaving port-*i* whereas V_j^+ is

the signal entering port-*j*, Specifically, the reflection coefficient (S_{11}) and transmission coefficient (S_{21}) give information about the amplitude and phase of the reflected power from port-1 and transmitted power (gain) from port-1 to port-2 of the vector network analyzer (VNA), respectively. The signal measured by VNA is directly proportional to electric and magnetic fields in the transmission line.

3. Experimental Setup and Data Acquisition

The layout of the experimental set-up is illustrated in Fig. 2(a). The experimental setup utilizes an Anritsu MS4640A VectorStar™ VNA which is controlled by a personal computer (PC). The VNA's port-1 signal feeds the 1500 W high power RF-PA which operates at the center frequency of 260 MHz. The detailed description of the setup is given in Table 2.

The power delivered to the load is sampled through the DC coupler (with attenuation 40 dB) which is in series with another 30 dB attenuator. Thus, total attenuation for the RF output power before being measured by the VNA's port-2 is 70 dB. The phase and amplitude of S_{11} (reflected signal) and S_{21} (transmitted signal) are recorded by the PC for each sample taken periodically during the experiment. The picture of the experimental setup is given in Fig. 2(b). The number of samples, sampling period, and the data acquisition (including the initialization and remote control of the VNA, adjustment of the power level, type of the output format i.e., Smith Chart as well as S_{11} and S_{21} measurements in log/linear scale selection etc.) are conditioned using testing software (TS) written in NI LabVIEW Software [12] (Fig. 3). TS also enables the instantaneous plots of the measured quantity on the available 4 windows in the user interface. Thus, in our experiments, the phase and amplitude of S_{11} and S_{21} for the most current sample can be observed by the operator. At the same time, these raw data obtained for each sample are recorded as a .txt file being automatically named by the TS. Finally, once all the samples are obtained, the acquired data are read from the recorded .txt files and are analyzed using MATLAB software [17].

4. Measurement Results

Once the test is run and all the samples are saved to the individual .txt files, the raw data are read by a prepared MATLAB script file. On the other hand, TARLA has a water cooling system controlled by a SCADA system which is also used to follow the water parameters (temperature, pressure with time stamp) on-line. The water

temperature data are kept in this system in weekly periods. The MATLAB script is also used to extract the time stamps of the recorded .txt files which include the phase and amplitude of S_{11} and S_{21}. Then, variation of S-parameters, temperature and pressure as a function of time can be observed together.

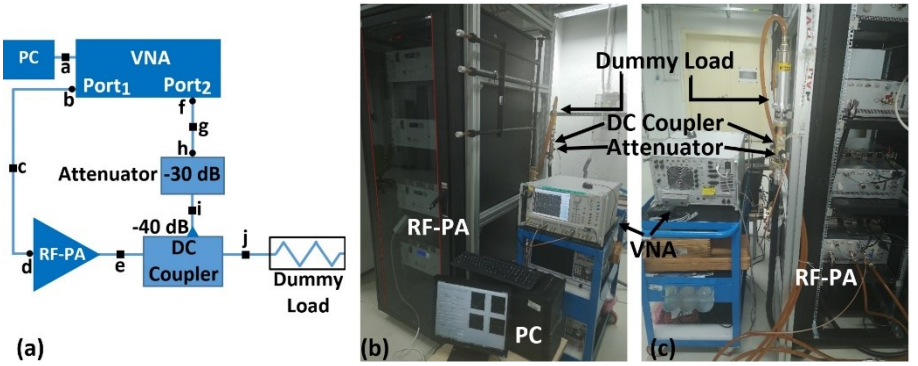

FIGURE 2. a) Block diagram of the experimental setup (ES), b) Picture of ES (Front side view), (c) Picture of ES (Back side view).

To avoid the spontaneous power shut down at the output of RF-PA which occurs due to the interlock as a result of fluctuation of the excitation signal, output signal of VNA from port-1 is set deliberately to relatively a lower value (-2 dBm) less than the maximum input signal capability of the RF-PA, which is 0 dBm. This setting yields ~1200 W output power from the RF-PA. One more reason for the selection of 1200 W is that the power which will be sent to SHB during real operation is also 1200 W. In this configuration, the reflected power shown on the display of the RF-PA is ~5 W. Leaks from connection points and cable ends, bending of high power RF cable for aligning it to its operation position act as both reflection and leakage points. These can cause increase in the reflected power and decrease in the delivered power.

In the first run of the experiment, we took 2794 many samples which resulted in a ~50-hour measurement. The reflection and transmission data obtained in this experiment are plotted in Fig. 4 thru Fig. 6 together with the plot of water temperature (on the right-hand side axis) as a function of time to examine the effect of water temperature on the response of the experimental setup.

Time information of all activities such as maintenance and system upgrade, etc. that interact with the water cooling line was recorded manually. The vertical red dash-

dotted lines, from 1 to 7, in Figs. 4 and 5 show such recorded interferences with the water cooling line at different time instants during the test. For instance, the chillers were being commissioned in the vicinity of time instants that are pointed out by lines 1 and 2. In the time interval in which line 3 resides, the pressure of force manifold varied and line 4 is to mark the time instant that the pressure of lift manifold was increased.

TABLE 2. Apparatus description for the experimental setup.

Label	Type	Description
a	cable	Standart USB cable.
b	port	Port-1 of VNA; N-type female.
c	cable	RG142 RF, N-type male connectors on both ends; 2 m long; with an N-type female adapter on the VNA side.
d	port	Input port of RF-PA, N-type female.
e	cable	LCF78-50JA low loss, phase stable, high power RF cable, 7/8" male connectors on both ends with 7/16" female connector at RF-PA side and 15/8" EIA at DC Coupler side.
f	port	Port-2 of VNA; N-type female.
g	cable	RG142 RF N-type male connectors on both ends; 10 m long; with an N-type female adapter on the VNA side.
h	port	Output port of 30 dB attenuator; N-type male.
i	connection	Direct series connection between the 30 dB attenuator and the sampling ouput port (N-type female) of the DC coupler.
j	connection	Direct series connection (1-5/8" EIA) between the ouput port of the DC coupler and the dummy load which is cooled down with water that is run through the water cooling system.

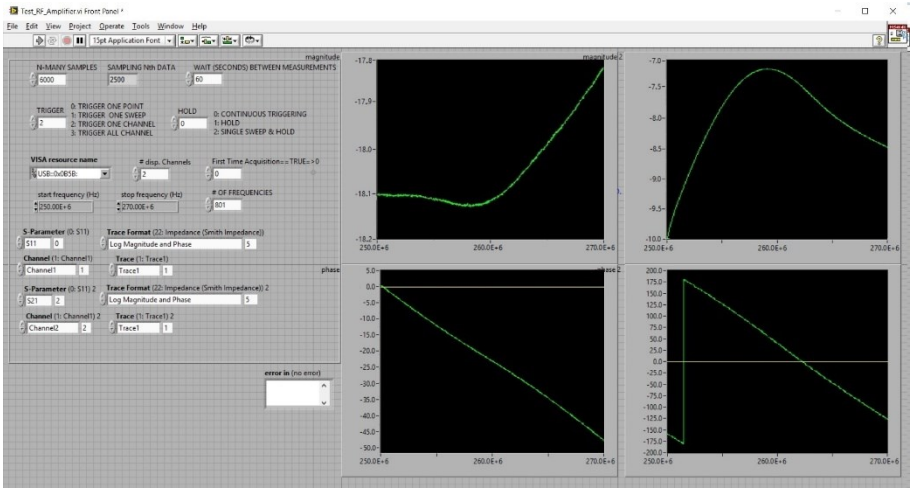

FIGURE 3. NI LabVIEW user interface which can control the VNA remotely, initialize the test, and save test data.

Line 5 indicates the pressure fluctuation in the water cooling line. The pressure level drop of the water cooling line becomes evident at the time instant that line 6 indicates. Maintenance was being performed around the time instant 7.

1200 W (~+60.79 dBm) output power of RF-PA is also verified with another digital power meter (R&S®NRP2 model). After attenuating this output power by 70 dB to protect the VNA, the power which is sampled by the VNA's port-2 becomes ~-9.21 dBm. Remembering that the input signal is -2 dBm, $|S_{21}|$ for the RF-PA should be measured as ~-7.21 dB (~-9.21 dBm-(-2 dBm)). This is in accordance with the experimental result given in Fig. 5(a) where $|S_{21}|$ is measured as ~-7.16 dB at steady state.

Large ripples in the magnitude and phase of S_{11} are evident in Fig. 4(a) and Fig. 4(b), respectively. These fluctuations are also observed in the magnitude and phase plots of S_{21} at the same time instants (Fig. 5(a) and Fig. 5(b)). Accordingly, it can be deduced that all pressure fluctuations at the input through the water cooling line will reflect as large ripples in the magnitude and phase of the output power. The water-cooling operation temperature of the amplifier is seen to slightly vary around 19.4°C in Fig. 5. In addition to the effect of water line pressure, the phase graph of S_{21} in Fig. 5(b) illustrates that all temperature variations in water cooling line triggers the phase change at the output.

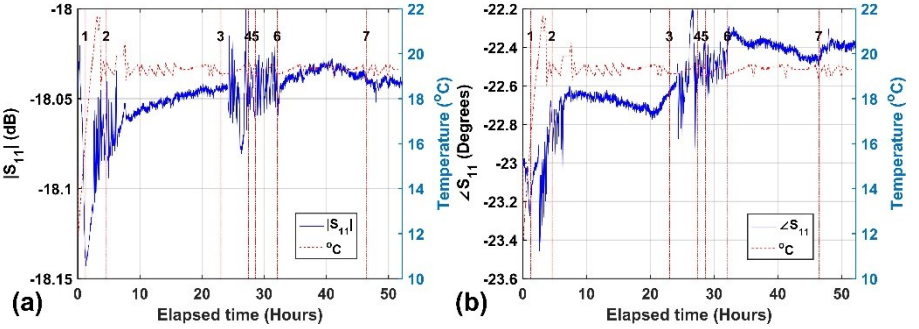

FIGURE 4. Measurement results of S_{11}. a) magnitude ($|S_{11}|$): (solid blue) b) phase ($\angle S_{11}$) (solid blue) together with water cooling line temperature (dashed red) on the right-hand side axis as a function of elapsed time in the experiment. Dash-dotted vertical lines are to show the selected time instants described in the text above.

As a result of Eqn. (1-5), it is desired to have minimum variation of phase in the output power. Under optimum conditions, i.e., with minimal variation in the water line temperature and pressure, one can see in Fig. 5(b) that there is a minimal phase variation between hours 15.5 and 21. Fig. 6 provides with a closer look at the mentioned situation in Fig. 5(b), presenting the phase variation of output power in the mentioned time interval between hour 15.5 thru hour 21. It is seen that the phase variation in this period is about 0.1 deg/0.2 °C ≈ 0.5 deg/°C.

These measurements were repeated several times and similar results were obtained. A representative of the repeated measurements is depicted in Fig. 7 and Fig. 8 using the results of another ~180-hour long measurement. In Fig. 8(a), again, $|S_{21}|$ converges to ~-7.17 dBm which is similar to the steady state value observed in Fig. 5(a). A closer view of S_{21} for the phase measurement in Fig.8 (b) is given in Fig. 9. The water cooling temperature plot is in line with the phase variation plot of S_{21}. Figure indicates a closer view for understanding this relationship.

The phase variation of output power around hour 95, which is considered to correspond to the most stable operation from Fig. 9, in the second measurement is about 0.4 deg/0.6 °C ≈ 0.67 deg/°C.

The variation in the output power's phase has made the following necessity evident for us as a result of the mentioned measurements above: requirement of integrating a phase shifter for the feeding circuit of the SHB to control the phase variation.

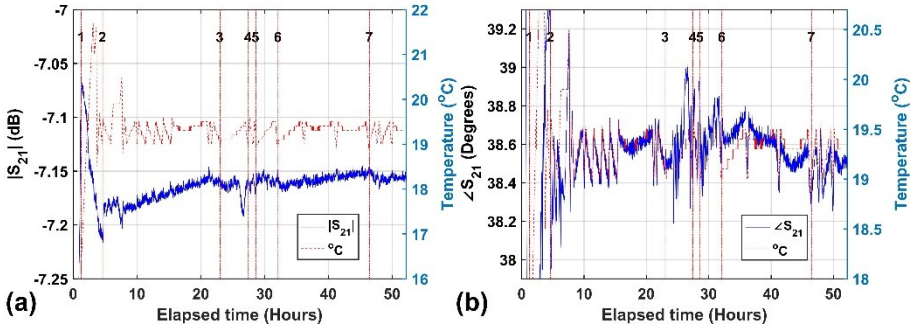

FIGURE 5. Measurement results of S_{21}. a) magnitude ($|S_{21}|$): (solid blue) b) phase ($\angle S_{21}$) (solid blue) together with water cooling line temperature (dashed red) on the right-hand side axis as a function of elapsed time in the experiment. Dash-dotted vertical lines are to show the selected time instants described in the text above.

5. CONCLUSION

The operation studies of SHB within the commissioning of injector line studies have been continuing and it is in accordance with the TARLA injector line commissioning scope.

This study shows that not only the temperature variations [18-20], but also the pressure stabilization of cooling (water) line is of importance for minimizing the phase variation of the output power of the amplifier. The effect of variation in the cooling line temperature on the magnitude and phase of S_{11} (i.e., the reflected power) as well as the magnitude of S_{21} (i.e., the transmitted power) is evident through Figs. 4-5(a). On the other hand, the effect of variation in the phase of S_{21} is more dominant in the performance of the overall system. Special attention to the variation in the phase of S_{21} should be paid. Based on the observations in this study, it is concluded that besides the necessity of stable temperature, keeping the pressure level of the cooling line constant has turned out to be important for phase stabilization in the output power for a 260 MHz RF-PA.

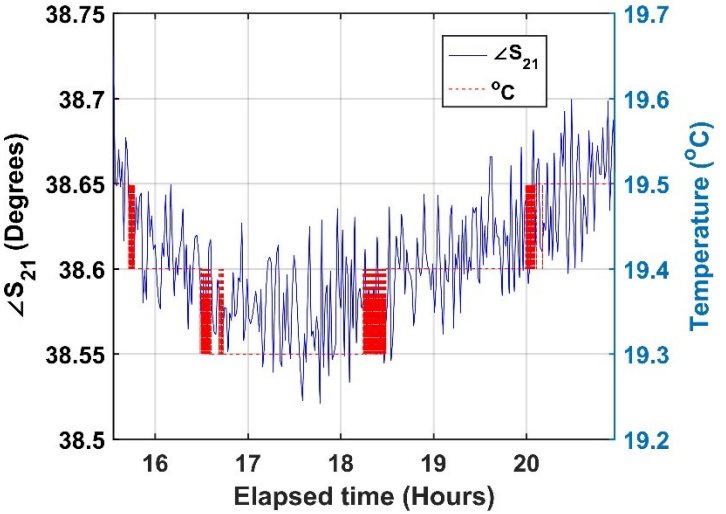

FIGURE 6. Phase variation of S_{21} ($\angle S_{21}$) (solid blue) and measured water cooling line temperature (dashed red) on the right-hand side axis, with a closer look for the situation in Fig. 5(b) within the time interval in between hour 15.5 and hour 21.

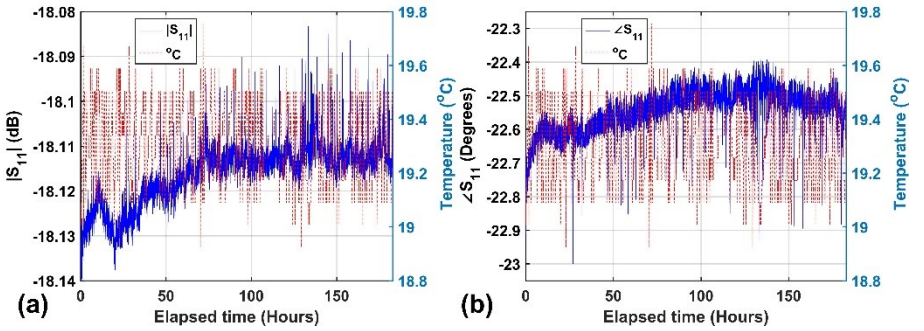

FIGURE 7. Measurement results of S_{11} a) magnitude ($|S_{11}|$) (solid blue) b) phase ($\angle S_{11}$) (solid blue) together with water cooling line temperature (dashed red) on the right-hand side axis as a function of elapsed time in the experiment.

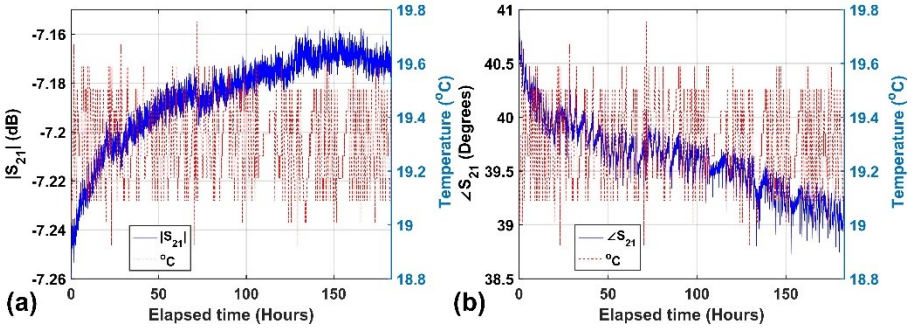

FIGURE 8. Measurement results of S_{21} a) magnitude ($|S_{21}|$) (solid blue) b) phase ($\angle S_{21}$) (solid blue) together with water cooling line temperature (dashed red) on the right-hand side axis as a function of elapsed time in the experiment.

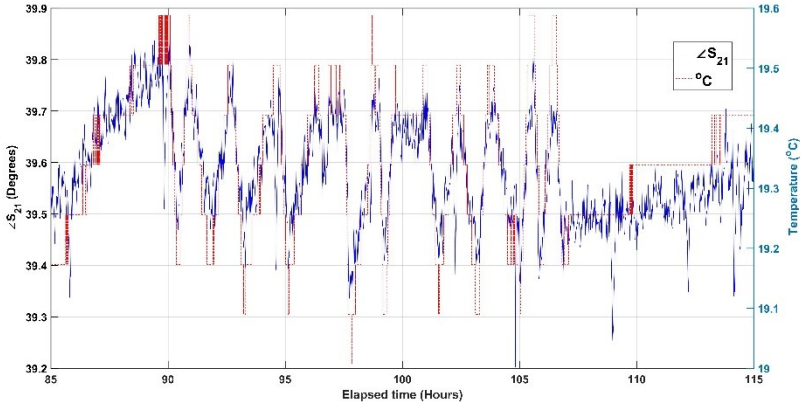

FIGURE 9. A closer view of S_{21} phase ($\angle S_{21}$) measurement borrowed from Fig. 8(b) in between hours 85 and 115: phase (solid blue) together with water cooling line temperature (dashed red) on the right-hand side axis as a function of elapsed time in the experiment.

The beam energy spread depends on RF phase and amplitude variations. Cooling temperature changes the beam energy indirectly. The long term beam energy drift and phase drift should be reduced by using accurate cooling control system. Furthermore, RF distributions for the injector system should be designed for maximal phase stability relative to the bunches in the linear accelerator [21].

In order to obtain the desired amplitude and phase stability in the accelerator structure in the presence of large perturbations such as beam loading or frequency shifts, it is necessary to use feedback control [22]. For this reason, the next step in the commissioning of the amplifier is the realization of the long-term operation of the complete system with the phase shifter and SHB, including the RF controller.

These tests will be performed in two stages: the first step will include the manual tuning of the phase shifter and in the second step, the long-term operation process will be carried out. The utilization of phase shifter will enable us to decrease the reflected power to the order of mWs, which is measured as ~5Ws in this study. After completion of the tests for the overall integrated system including RF-PA, SHB and RF controller, we aim to achieve the phase stability value of 0.35 deg/ºC as given in Table 1. This target seems feasible since the phase variation results which are the measured as 0.5 deg/ºC and 0.67 deg/ºC, are low enough to be corrected by RF controller which will be incorporated in near future.

Acknowledgments. This work is supported by Presidency Strategy and Budget Department under Grant No: 2006K-120470. The authors would like to thank to the TARLA team for their devoted work.

References

[1] Aksoy, A., Karslı, O. and Yavas, O., The Turkish accelerator complex IR FEL project, *Infrared Phys. Technol.,* 51/5 (2008) 378-81.

[2] Aksoy, A. and Karsli, O. (Eds.), The technical design report of Turkish Accelerator and Radiation Laboratory in Ankara, Technical Report (Ankara University, 2015).

[3] Aksoy, A., Karsli, O., Aydin, A., Kaya, C., Ketenoglu, B., Ketenoglu, D. and Yavas, O., Current status of Turkish Accelerator and Radiation Laboratory in Ankara: the TARLA facility, *Can. J. Phys.,* 96/7 (2018) 837-42.

[4] Karsli, O., Aksoy, A., Kaya, C., Koc, B., Dogan, M., Elcim, O.F. and Bozdogan, M., High power RF operations studies at TARLA facility, *Can. J. Phys.,* Accepted: https://doi.org/10.1139/cjp-2018-0778.

[5] Wangler, T.P., RF Linear accelerators, John Wiley & Sons, 2008.

[6] Karsli, O., Yavas, O. and Dogan, M., Design of L Band 20 kW High Power Solid State Amplifier for TARLA/TAC Project, *Известия высших учебных заведений. Физика.*, 55/10-3 (2012) 154-9.

[7] Karsli, O. and Yavas, O., A design study on high power RF system for the TARLA facility of TAC, *Nucl. Instrum. Methods Phys. Res. A*, 693 (2012) 215-9.

[8] Wang, F., Liu, K., Feng, L., Lin, L., Zhang, B., Hao, J. and Quan, S., Using a 1.3 GHz 20 kW Solid State Amplifier as RF Power Supply for DC-SRF Photo-injector, *6th Workshop on ERL,* New York, USA 2015.

[9] Dillon, S., Schach, C. and Nobel, B., Design of a high speed pulsed 324 MHz solid-state amplifier for use in a beam chopper, *IPAC2012*, Louisiana, USA, (2012) 2242-4.

[10] Frenzel, L.E., RF power for industrial applications, Pearson Prentice Hall 2004.

[11] SigmaPhi Accelerator Technologies, https://www.sigmaphi.fr/en/produits/amplificateurs-radiofrequence, Accessed: 2019-03-20.

[12] National Instruments, http://www.ni.com/en-tr/shop/labview/labview-details.html, Accessed: 22.03.2019.

[13] Wurlich, A., CERN Accelerator School, CERN-94-01, 1994.
[14] Wiedemann, H., Particle accelerator physics, (Vol. 314), Springer, Berlin, 2007.
[15] Chao, A.W., Handbook of Accelerator Physics and Engineering, 2nd Printing, World Scientific Publishing Co. Pte. Ltd., pp.256, 1998.
[16] Pozar, D. M., Microwave engineering, 4th Edition, John Wiley & Sons, 174 Chapter 4, 2011.
[17] MathWorks, https://www.mathworks.com/products/matlab.html, Accessed: 22.03. 2019.
[18] Akre, R., Temperature Stability of RF Components, (2005). http://slac. stanford.edu/grp/lcls/controls/global/subsystems/llrf/26sep2005Review/Temperature%20Stability%20of%20RF%20Components%20Apr%2005.pdf Accessed: 13.04.2019.
[19] Akre, R., Emma, P. and Krejcik, P., Measurements on SLAC LINAC RF system for LCLS Operation *PACS2001, Proceedings of the 2001 Particle Accelerator Conference (Cat. No. 01CH37268)*, 2 (2001) 1453-1455.
[20] Decker, F.J., Akre, R., Byrne, M., Farkas, Z.D., Jarvis, H., Jobe, K., Koontz, R., Mitchell, M., Pennacchi, R., Ross, M. and Smith, H., Effects of temperature variation on the SLC LINAC RF system, *IEEE Proceedings of Particle Accelerator Conference*, 3 (1995) 1821-1823.
[21] MAX IV Detailed Design Report, https://www.maxiv.lu.se/accelerators-beamlines/accelerators/accelerator-documentation/max-iv-ddr Accessed: 13.04. 2019.
[22] Suelzle, L.R., RF amplitude and phase stabilization for a superconducting linear accelerator by feedback stabilization techniques, High Energy Physics Lab, (1968), https://www.bnl.gov/magnets/staff/gupta/Summer1968/0067.pdf Accessed: 22.03. 2019.

Current Address: Ozlem Karsli: Institute of Accelerator Technologies, Ankara University 06830, Gölbaşı, Ankara, TURKEY
E-mail: okarsli@ankara.edu.tr,
ORCID: https://orcid.org/0000-0002-1466-4989

Current Address: Evrim Colak (corresponding author): Institute of Accelerator Technologies, Ankara University, 06830, Gölbaşı, Ankara, TURKEY
Electrical and Electronics Engineering Department, Ankara University, TURKEY
E-mail: evrim.colak@ankara.edu.tr
ORCID: https://orcid.org/0000-0002-4961-5060